Voxel-based statistical analysis of cerebral glucose metabolism in the rat cortical deafness model by 3D reconstruction of brain from autoradiographic images

Jae Sung Lee[1, 2], Soon-Hyun Ahn[3], Dong Soo Lee[1], Seung Ha Oh[3], Chong Sun Kim[3], Jae Min Jeong[1], Kwang Suk Park[1, 2], June-Key Chung[3], Myung Chul Lee[3]

[1] Department of Nuclear Medicine, Seoul National University College of Medicine, 28 Yungun-Dong, Chongno-Ku, Seoul 110-799, Korea
[2] Department of Biomedical Engineering, Seoul National University College of Medicine, Seoul, Korea
[3] Department of Otolaryngology, Head and Neck Surgery, Seoul National University College of Medicine, Seoul, Korea

Received: 27 September 2004 / Accepted: 19 November 2004 / Published online: 4 March 2005

Abstract. *Purpose:* Animal models of cortical deafness are essential for investigation of the cerebral glucose metabolism in congenital or prelingual deafness. Autoradiographic imaging is mainly used to assess the cerebral glucose metabolism in rodents. In this study, procedures for the 3D voxel-based statistical analysis of autoradiographic data were established to enable investigations of the within-modal and cross-modal plasticity through entire areas of the brain of sensory-deprived animals without lumping together heterogeneous subregions within each brain structure into a large region of interest.
Methods: Thirteen 2-[1-^{14}C]-deoxy-D-glucose autoradiographic images were acquired from six deaf and seven age-matched normal rats (age 6–10 weeks). The deafness was induced by surgical ablation. For the 3D voxel-based statistical analysis, brain slices were extracted semiautomatically from the autoradiographic images, which contained the coronal sections of the brain, and were stacked into 3D volume data. Using principal axes matching and mutual information maximization algorithms, the adjacent coronal sections were co-registered using a rigid body transformation, and all sections were realigned to the first section. A study-specific template was composed and the realigned images were spatially normalized onto the template. Following count normalization, voxel-wise *t* tests were performed to reveal the areas with significant differences in cerebral glucose metabolism between the deaf and the control rats.
Results: Continuous and clear edges were detected in each image after registration between the coronal sections, and the internal and external landmarks extracted from the spatially normalized images were well matched, demonstrating the reliability of the spatial processing procedures. Voxel-wise *t* tests showed that the glucose metabolism in the bilateral auditory cortices of the deaf rats was significantly ($P<0.001$) lower than that in the controls. There was no significantly reduced metabolism in any other area, and no area showed a significant increase in metabolism in the deaf rats with the same threshold, demonstrating the high localization accuracy and specificity of the method developed in this study.
Conclusion: This study established new procedures for the 3D reconstruction and voxel-based analysis of autoradiographic data which will be useful for examining the cerebral glucose metabolism in a rat cortical deafness model.

Keywords: Autoradiography – Cerebral glucose metabolism – Voxel-based analysis – Deafness – Rat

Eur J Nucl Med Mol Imaging (2005) 32:696–701
DOI 10.1007/s00259-004-1739-y

Dong Soo Lee (✉)
Department of Nuclear Medicine, Seoul National University College of Medicine, 28 Yungun-Dong, Chongno-Ku
Seoul 110-799, Korea
e-mail: dsl@plaza.snu.ac.kr
Tel.: +82-2-7602501, Fax: +82-2-7457690

Introduction

Investigations into the cerebral glucose metabolism in patients with cortical deafness using ^{18}F-fluorodeoxyglucose (FDG) positron emission tomography (PET) have reported abnormal glucose metabolism in the auditory cortex and related areas [1–5]. In both prelingual and postlingual deafness, the glucose metabolism in these areas has been found to be lower than that in normal controls. However, the decreased metabolism gradually recovers and may even exceed the normal level of metabolism. These findings appear to be due to the reorganization of neuronal networks in these areas [2–7]. In most investigations into FDG brain PET images from deaf children and adolescents which have

examined the dynamics of glucose metabolism in the developing stage, the results may have been confounded by the effects of age on account of the unavailability of PET data acquired from age-matched normal controls [4]. These limitations in human PET studies are due to ethical considerations, which highlights the need for animal cortical deafness models and the development of techniques for analysis of the brain images of these animals.

Although dedicated animal PET and single-photon emission computed tomography (SPECT) systems with a high resolution and sensitivity have been developed and used to perform in vivo imaging studies of small live animals [8–11], autoradiographic imaging is still a powerful and predominantly used tool for quantification of the radioisotope distribution in small animals, such as rats and mice. Voxel-based analysis of tomographic images, such as statistical parametric mapping (SPM), is widely used for examination of brain PET and SPECT data [12]. However, it is rarely applied to autoradiographic images. From autoradiographic images, the regional activity concentration of the radioisotope is still obtained by manually drawing a region of interest (ROI) or by using a predefined ROI on a brain atlas. However, SPM-like voxel-based analysis of autoradiographic data is important for investigation of the within-modal and cross-modal plasticity in the brain of sensory-deprived animals because every part of the brain should be tested and the subregions within each brain structure should not be lumped into large ROIs [4, 5].

The aim of this study was to establish procedures for reconstructing three-dimensional (3D) images and voxel-based analysis of the autoradiographic data, and to determine whether this approach is useful for investigation of the cerebral glucose metabolism in a rat cortical deafness model[1].

Materials and methods

Animal model for deafness and autoradiography

Autoradiographic studies that were obtained from a companion study conducted in our laboratory were used. Only the data acquired from six deaf and seven control rats for which the autoradiographic studies were performed between 4 and 8 weeks after surgery were analyzed in this study. This period is equivalent to a 3- to 6-year-old child, which is regarded as a critical age for treating prelingual deafness [14, 15]. After this period, the function of the auditory cortex may be altered by the neuronal plasticity, and the glucose metabolism in these areas appears to recover to a normal level [4, 14].

Bilateral cochleae were ablated surgically 10–14 days after birth to produce the animal model for deafness. The fluid in the cochlea was removed with a needle suction tip following a posterior auricular incision and suction of the mesodermal tissue in the middle ear. In the normal control rats, sham operations including only a skin incision and identification of the bulla surface were performed.

For the autoradiographic studies, the rats received 16 μCi/100 g of 2-[1-^{14}C]-deoxy-D-glucose (Perkin-Elmer, in an aqueous solution, 56 mCi/m*M*) intraperitoneally, and were exposed to a quiet environment without occlusion of the ears. The animals were decapitated, and the brains were removed and frozen immediately. Serial coronal sections of the brain with a thickness of 20 μm were cut from the frontal lobe to the inferior colliculus level. Every six sections were collected on a microscope slide glass after discarding the five sections between them. Therefore, the distance between the axial centers of the collected sections was 120 μm. The slides were dried for 1 day and exposed to an autoradiographic image plate (Bioimage Analyzing System, Fujifilm) for 5 or 6 days, and the digitized images, the pixel value of which was proportional to the cerebral glucose metabolism, were acquired using an FLA-2000 scanner (Fujifilm). The voxel size of the image was 50×50 μm.

Image analysis procedures

Figure 1 shows the procedures for analyzing the autoradiographic images for the 3D voxel-based statistical analysis used in this study. First, the slices were extracted from the autoradiographic images, which contained the coronal sections of a rat brain. Second, the adjacent slices were realigned to each other two-dimensionally (2D) using principal axes matching and mutual information maximization algorithms [16, 17]. Third, the realigned 2D slices were stacked to reconstruct the 3D volume data. Fourth, a study-specific template was composed and all the individual images were spatially normalized into the template image. Finally, voxel-wise statistical analysis was performed. The details for each data processing step are given in the following sections.

Slice extraction and image registration

For the slice extraction procedure, the size of autoradiographic images was reduced by a factor of 8 to yield a matrix size of 1,010×512 (pixel size 400×400 μm) because this procedure does not require a fine image resolution. The original image (matrix size 8,080×4,096, pixel size 50×50 μm) was too large to be displayed on a computer monitor screen, and lower pixel numbers can reduce the processing time (Fig. 2a). The reduced 2D autoradiographic images were smoothed by convolution with an isotropic Gaussian kernel with 2 mm full-width at half-maximum (FWHM) (Fig. 2b). Without smoothing of images, small blobs due to noise in the background region were sometimes detected when the thresholding method was

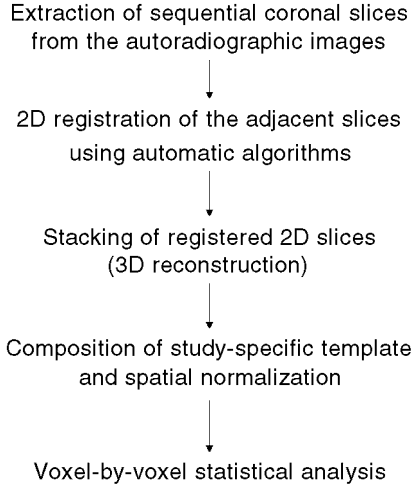

Fig. 1. Procedures for the analysis of the autoradiographic images used in this study for the 3D voxel-based statistical analysis.

[1]Results of a similar but independent investigation were recently reported by another group in ref. [13]

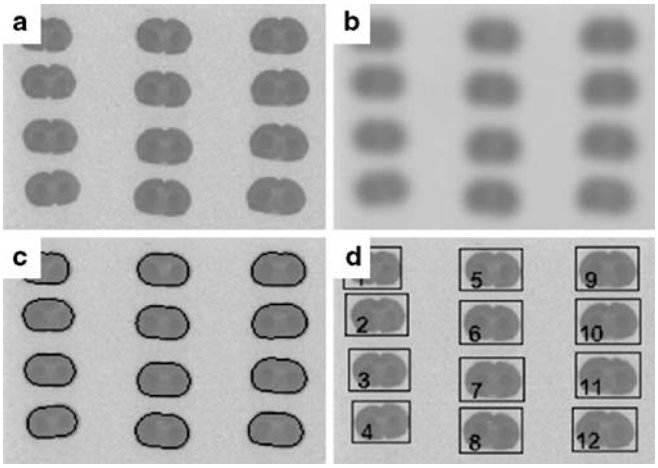

Fig. 2. The procedures for extracting the coronal sections from an autoradiographic image. **a** 2D autoradiographic image reduced by a factor of 8 (pixel size =400×400 μm). **b** Image smoothed by convolution with an isotropic Gaussian kernel with 2 mm FWHM. **c** Brain slices extracted using a threshold method. **d** The finally determined coronal sections and region indices labeled semi-automatically.

applied. Any low-pass filter could be used for this purpose. The Gaussian filter was selected as easy implementation of this filter in the spatial domain was possible. In addition, the slice extraction was not sensitive to the degree of smoothness if the FWHM value was within the range of 1–3 mm (approximately 3–7 times the pixel size). The brain slices were extracted from the smoothed image using a thresholding method in which the pixels with a higher gray level than a certain threshold were classified into brain slices and the others into background (Fig. 2c). A global threshold was used and adjusted to between 30% and 60% of the maximum pixel value in the smoothed image. Initially the threshold was set to 30%. The threshold was increased in increments of 5% if any of the neighboring slices had merged due to an insufficiently low threshold. A binary image was generated as a result of the thresholding, in which the pixels that belonged to the brain slices had a pixel value of 1 and those that belonged to the background had a value of 0.

A region-growing method was applied to the binary image in order to assign a unique region index to each separate blob (each brain section or background) [18]. The region with the largest area was determined to be the background and was not further analyzed. Around the other regions containing the brain slice, slightly larger rectangular boxes than their boundary (three more pixels from the *x*-extreme and *y*-extreme of the boundary) were drawn, as shown in Fig. 2d. The slice number was then assigned manually to each bounding box. The region indices assigned automatically using a region-growing algorithm were not used because the brain slice was not positioned in a consistent way by the investigators. The matrix size of the bounding boxes was approximately 40×30. Finally, the rectangular regions within the bounding box were sampled from the original large image and stacked into the 3D volume data that had a matrix dimension of 360×360×(number of slices) voxels (50×50×120 μm). File format of Analyze-7 (Mayo Clinic, Rochester, USA) was used to save the 3D volume data.

Sequential image registrations of the adjacent slices were performed using principal axes matching and mutual information maximization techniques for the coarse and the fine registration, respectively [16, 17]. The registration parameters obtained by the principal axes matching were used as the initial values for the mutual information maximization method in order to reduce the likelihood of encountering a local maximum during the search for the best transformation parameters. Image registration algorithms based on the similarity of the image intensity, such as the mutual information maximization method, are not limited by segmentation errors (as in the surface-based methods) and do not require the interaction of an operator (as in the point landmark-based methods). The most widely used similarity criteria include the sum of absolute differences, correlation coefficient, and mutual information of the joint intensity histogram. Among these similarity criteria, mutual information was selected in this study as this is a well-validated method for robust registration of autoradiographic images [19].

Only a rigid body transformation between the adjacent slices was allowed, and transformation matrices were calculated using the four registration parameters (translation in *x*-direction and *y*-direction, and rotation along the *x*-axis and *y*-axis). A transformation matrix between each slice and the first slice was obtained by multiplying the transformation matrices sequentially, and all the slices were realigned to the first slice. IDL-language (Research Systems Inc., Boulder, CO, USA) was used to implement the slice extraction and image registration procedures.

Spatial normalization and statistical analysis

For the voxel-based statistical analysis, the image volume data need to be transformed into standardized 3D coordinate space in order to remove the gross and detailed differences in the brain shape and orientation (spatial normalization) [20–22]. To facilitate the spatial normalization procedures, the image contrast was enhanced by subtracting half of the maximum voxel value in all voxels and rescaling the images from zero to the maximum value. Using this adjustment, the background noise was eliminated and the contrast within the cortical regions was significantly enhanced. Without the subtraction and rescaling processes, the boundaries of brain slices in some cases were not matched with the boundary of the target image. Each image slice was then rebinned into 120×120 matrix (150× 150 μm) to make the data more isotropic and to reduce the burden of the calculation.

An image of a normal rat was selected as the reference target volume and was smoothed by convolution using an isotropic Gaussian kernel with 800 μm FWHM. The other images were then spatially normalized onto the target volume using linear and non-linear transformations [20, 21], and averaged after intensity normalization by proportional scaling to generate a study-specific template image [23]. The template image was smoothed and all the images were spatially normalized onto the template image again. The voxel size of the spatially normalized images was 150×150×150 μm.

The spatially normalized images were smoothed using a Gaussian kernel with 800 μm FWHM, and a voxel-wise *t* test was then performed to identify the regions with significantly different voxel counts between the normal and the deaf rats ($P<0.001$) following count normalization using proportional scaling. The aims of smoothing were to increase the signal-to-noise ratio, to conform the data more closely to Gaussian distribution, and to account for variations in the subtle anatomical structures. The kernel size of 800 μm was used since the expected resolution of the spatially normalized images was ~300 μm (two times the voxel size) and a kernel size of 2–4 times the spatial resolution has been used in human studies. The SPM99 program was used for the spatial normalization, image smoothing, and statistical analysis [12, 20, 21].

Comparison with ROI analysis

For comparison of the findings obtained by voxel-based analysis with the conventionally used ROI-based method, ROIs were drawn on the auditory cortex, motor cortex, somatosensory cortex, visual cortex, caudate putamen, thalamus, hippocampus and amygdalae in

both hemispheres using the Paxinos rat brain atlas as a reference [24]. The regional mean pixel value in each ROI was normalized to the mean count of whole brain, and group mean comparison between the normal and deaf rats was performed using a *t* test. SPSS 10.0 was used.

Results

The transaxial slices shown in Fig. 3 were obtained by reslicing the reconstructed 3D volume data of a rat brain that were generated by stacking the coronal sections before (Fig. 3a) and after registration (Fig. 3b) of the adjacent slices using a rigid body transformation for which the mutual information between the images was used as an optimization criteria. After applying the image registration, the saw-toothed pattern on the brain surface of the transaxial slice, as shown in Fig. 3a, was eliminated and the boundaries of the internal brain structures, such as the caudate putamen and internal capsule, became more obvious (Fig. 3b). The contrast of the images shown in Fig. 3 was enhanced to eliminate the background noise and make the boundaries easier to identify.

The boundaries of the brain surface and the internal capsule were extracted from a transaxial slice of each spatially normalized image by looking for the local maxima of the gradient of the image intensity [25] and superimposed on the template image to show the accuracy of the spatial normalization process (Fig. 4). The overlap of the boundaries, which subsumed the spatial normalization error, the uncompensated morphological difference among individual brains, and the uncertainty in the edge extraction algorithm, was coded using a hot-metal colormap, i.e., increasing the overlap from dark brown to white. Figure 4 shows the high accuracy in matching the brain surface and the internal capsule. Although the boundary of the internal capsule showed a higher variability than the brain surface, it would still be acceptable considering the size of the neighboring cortical and subcortical structures of the rat brain.

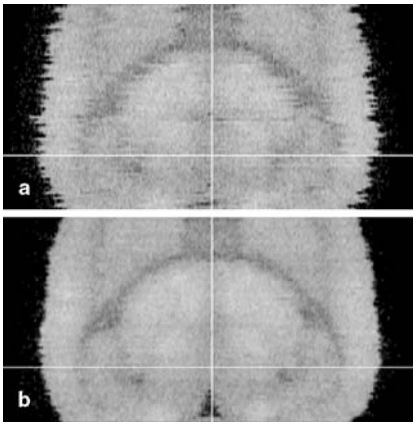

Fig. 3. Transaxial slices obtained by reslicing the reconstructed 3D volume data generated by stacking the coronal sections. **a** Before image registration of the adjacent slices using a rigid body transformation. **b** After image registration.

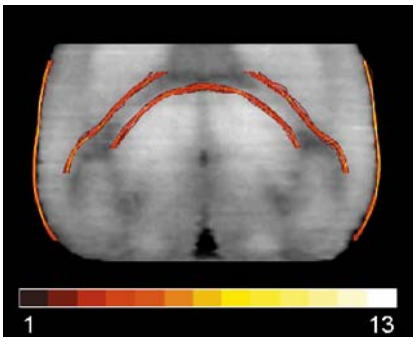

Fig. 4. Boundaries of the brain surface and internal capsule extracted from a transaxial slice of each spatially normalized image and superimposed on the template image. Overlap of the boundaries was coded using a hot-metal colormap increasing the overlap from dark brown to white.

When the spatially normalized autoradiographic images of deaf rats were compared with those of the normal controls by performing a *t* test at each voxel, after removing the effects of the global count, the glucose metabolism in the bilateral auditory cortices of the deaf rats was significantly ($P<0.001$) lower than that of the controls. The significantly reduced metabolism was not observed in any area other than the auditory cortex, and no area showed a significant increase in metabolism in the deaf rats with the same threshold, which demonstrates the high localization accuracy and specificity of the method presented in this study. The brain areas with a significantly reduced glucose metabolism in the deaf rats are shown in Fig. 5, where a threshold of $P<0.01$ rather than $P<0.001$ has been used for display purpose. When $P<0.01$ was applied, there was again no significant increase in metabolism.

ROI analysis also showed significant reduction of glucose metabolism only in both auditory cortices of deaf rats when the same threshold ($P<0.001$) was applied ($T= 7.34$ in the right hemisphere, $T=7.91$ in the left hemisphere), verifying the reliability of the voxel-based analysis.

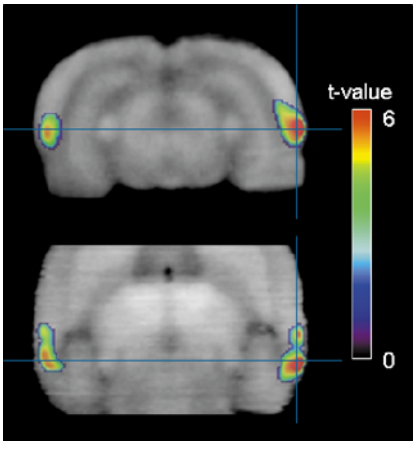

Fig. 5. Brain areas with a significantly decreased glucose metabolism in deaf rats compared with the age-matched normal controls ($P0.01$). The *top image* shows a coronal slice and the *bottom image*, a transaxial slice.

Discussion

Three-dimensional reconstruction of the brain from the serial sections of the autoradiographic images allows investigators to observe the sectional planes and outer surfaces from any viewing angle and to make quantitative volumetric analyses [19, 26–29]. Co-registration of the 3D reconstructed autoradiographic images with other tomographic images, such as PET, SPECT, computed tomography (CT) and magnetic resonance imaging (MRI), is also required for correlative studies between the different imaging modalities and the performance evaluation of the newly developed animal PET and SPECT scanners. The ability to quantify the radioactivity distribution using animal PET and SPECT scanners needs to be verified by comparing the in vivo images with the findings from the autoradiographic images. Another purpose may be to map the autoradiographic images into the anatomical reference systems in order to associate them with standardized atlas structures and analyze the data statistically at a voxel level using SPM-like techniques [13, 30, 31]. SPM-like analysis of the brain PET, SPECT, and autoradiographic images of rodents will facilitate investigations into the brain function and anatomy of these animals in a common anatomic space [32], which can be extended to human studies. This will accelerate the transition of any new discoveries from animal studies to human applications because such voxel-based analysis is widely performed for human data. Since the animal PET and SPECT scanners have a spatial resolution in the order of millimeters, it is still not certain that SPM-like analysis of these images will provide sufficient and correct information regarding the location and extent of the abnormal regions and activated areas.

The fundamental prerequisite for a 3D reconstruction of autoradiographic images is a 2D image registration of each slice image to (1) the video reference images of the remaining uncut specimen's block face recorded during the cryomicrotome procedure prior to sectioning, or (2) its adjacent slices [19, 26–28]. Despite its strong potency to reduce any possible deformation artifacts of the slices associated with the slice sectioning, reconstruction by registering each slice to the video reference images has not been used widely because it requires additional devices in order to acquire the video images [19]. Therefore, 3D reconstruction methods via the registration of the adjacent slices using linear or nonlinear image registration techniques are generally used [26–28]. This study used a two-step approach: fine image registration using the mutual information maximization method following a coarse registration using principal axes matching [16, 17]. Although the principal axes matching method works rapidly and provides an approximate solution for optimal image matching, the principal axes alignment is unsatisfactory if the image is almost round or if it has no symmetry [26, 27]. Therefore, the solution of the principal axes matching method was only used as an initial guess in order to determine the optimal transformation parameters by the mutual information maximization method.

In the image registration process, only the rigid body transformation between adjacent coronal sections was allowed. This restriction in the transformation relies on the assumption that the radioactivity distribution changes gradually across the adjacent sections and that the coronal sections are negligibly deformed during the autoradiographic procedures. Although the data sometimes exhibit such global and regional deformation artifacts as a result of species sectioning and tissue shrinkage [19], linear and/or nonlinear deformation between the adjacent sections can distort the brain structures, particularly in the slices where the radioactivity distribution alters abruptly across the coronal sections. Therefore, it is better to preserve the shape of each section without compensating for the deformation than to take the risk of distorting the global and regional image information during the registration process.

Spatial normalization of the images into the template accounts not only for the intersubject variability in the brain anatomy but also to some extent for such deformation in the individual slices. Although Zhao et al. [30] suggested the transformation of autoradiographic images into standard anatomical space [31], they only applied a 2D affine transformation to the in-plane spatial normalization of the individual coronal section and matched the section with a corresponding coronal slice in the template, which was located at the same anteroposterior distance from the common coronal reference level (+0.7 mm from the bregma). The arbitrariness in determining the common reference plane, the lack of anatomical standardization in the anteroposterior direction, and the insufficient compensation for the regional anatomical variability by using only the 2D affine transformation might be limitations of their pioneering studies.

The underlying assumption in employing the anatomical standardization of an individual brain is that the intersubject anatomical variability should be within the range of the values expected by the spatial normalization algorithm. This assumption would be reasonable since the brain anat omy of rats with a corresponding weight is quite similar, even for different genders and strains [24, 32]. In addition, a study-specific template was used in this study, which was generated by averaging the individual images spatially normalized onto an initial target brain; this was done in order to minimize the error in the registration between the source images and template due to the possible singularity in the selected target brain, and to force the transformation parameters to have a Gaussian distribution by using the average image as a spatial normalization target [22, 23]. Figure 4 shows the boundaries of the brain surface and internal capsule extracted from the transaxial plane resliced from the individual spatially normalized images. The continuity and consistency of these boundaries demonstrate the success of the spatial normalization process due to the reasonable assumptions and appropriate strategies used in this study as well as to the accuracy in image registration between the coronal sections.

In this study, the cerebral glucose metabolism of the rats with deafness and the age-matched controls was measured

by autoradiography, and these autoradiographic imaging data were analyzed using the presented methods. A rat cortical deafness model is an excellent model for verification of this approach using the 3D reconstruction of autoradiographic images and SPM-like voxel-based analysis because the reduced glucose metabolism may be localized to the auditory related cortices, which are known to be specifically affected by a deficiency in the auditory input signal [1–5]. The statistical parametric map of the *t* value, which is the final product of this study, showed a bilateral decrease in glucose metabolism, which was localized to the auditory cortex of the rat brain (Fig. 5). In addition, no area with increased metabolism was detected: if it were to exist, it is likely that such a finding would be due to errors in the processing step, considering the previous findings in human studies [5].

Conclusion

This study established new procedures for the 3D reconstruction and voxel-based analysis of autoradiographic data which will be useful for examining the cerebral glucose metabolism in a rat cortical deafness model.

Acknowledgements. This work was supported in part by the Korean Science and Engineering Foundation (Grant No. R01-2002-000-00346-0) and in part by BK21 Human Life Sciences.

References

1. Ito J, Sakakibara J, Iwasaki Y, Yonekura Y. Positron emission tomography of auditory sensation in deaf patients and patients with cochlear implants. Ann Otol Rhinol Laryngol 1993;102: 797–801.
2. Catalán-Ahumada M, Deggouj N, De Volder A, Melin J, Michel C, Veraart C. High metabolic activity demonstrated by positron emission tomography in human auditory cortex in case of deafness of early onset. Brain Res 1993;623:287–92.
3. Deggouj N, Devolder A, Catalan M, Melin J, Michel C, Gersdorff M, et al. Positron emission tomography in deaf patients at rest. Adv Otorhinolaryngol 1995;50:31–7.
4. Lee DS, Lee JS, Oh SH, Kim SK, Kim JW, Chung JK, et al. Cross-modal plasticity and cochlear implants. Nature 2001;409: 149–50.
5. Lee JS, Lee DS, Oh SH, Kim CS, Kim JW, Hwang CH, et al. PET evidence of neuroplasticity in adult auditory cortex of postlingual deafness. J Nucl Med 2003;44:1435–9.
6. Bavelier D, Neville HJ. Cross-modal plasticity: where and how? Nature Rev Neurosci 2002;3:443–52.
7. Cordes M, Wszolek ZK. Deafness and cerebral plasticity. J Nucl Med 2003;44:1440–2.
8. Ishizu K, Mukai T, Yonekura Y, Pagani M, Fujita T, Magata Y, et al. Ultra-high resolution SPECT system using four pinhole collimators for small animal studies. J Nucl Med 1995;36: 2282–7.
9. Weber DA, Ivanovich M. Pinhole SPECT: ultra-high resolution imaging for small animal studies. J Nucl Med 1995; 36:2287–9.
10. Chatziioannou AF. Molecular imaging of small animals with dedicated PET tomographs. Eur J Nucl Med Mol Imaging 2002; 29:98–114.
11. Lewis JS, Achilefu S, Garbow JR, Laforest R, Welch MJ. Small animal imaging. Current technology and perspectives for oncological imaging. Eur J Cancer 2002;38:2173–88.
12. Friston KJ, Holmes AP, Worsley KJ, Poline J-P, Frith CD, Frackowiak RSJ. Statistical parametric maps in functional imaging: a general linear approach. Hum Brain Mapp 1995;2: 189–210.
13. Nguyen PT, Holschneider DP, Maarek JM, Yang J, Mandelkern MA. Statistical parametric mapping applied to an autoradiographic study of cerebral activation during treadmill walking in rats. Neuroimage 2004;23:252–9.
14. Ahn SH, Oh SH, Lee JS, Jeong JM, Lim D, Lee DS, et al. Changes of 2-deoxyglucose uptake in the rat auditory pathway after bilateral ablation of the cochlea. Hear Res 2004; 196:33–8.
15. Sharma A, Dorman MF, Spahr AJ. A sensitive period for the development of the central auditory system in children with cochlear implants: implications for age of implantation. Ear Hear 2002;23:532–9.
16. Alpert NM, Bradshaw JF, Kennedy D, Correia JA. The principal axes transformation—a method for image registration. J Nucl Med 1990;31:1717–22.
17. Maes F, Collignon A, Vandermeulen D, Marchal G, Suetens P. Multimodality image registration by maximization of mutual information. IEEE Trans Med Imaging 1997;16:187–98.
18. Gonzalez RC, Woods RE. Digital image processing. Reading, MA: Addison-Wesley; 1992. p. 458–61.
19. Kim B, Boes JL, Frey KA, Meyer CR. Mutual information for automated unwarping of rat brain autoradiographs. Neuroimage 1997;5:31–40.
20. Friston KJ, Ashburner J, Frith CD, Poline J-B, Heather JD, Frackowiak RSJ. Spatial registration and normalization of images. Hum Brain Mapp 1995;2:165–89.
21. Ashburner J, Friston KJ. Nonlinear spatial normalization using basis functions. Hum Brain Mapp 1999;7:254–66.
22. Toga AW, Thompson PM. Maps of the brain. Anat Rec 2001; 265:37–53.
23. Karas GB, Burton EJ, Rombouts SA, van Schijndel RA, O'Brien JT, Scheltens P, et al. A comprehensive study of gray matter loss in patients with Alzheimer's disease using optimized voxel-based morphometry. Neuroimage 2003;18: 895–907.
24. Paxinos G, Watson C. The rat brain in stereotaxic coordinates. Orlando, FL: Academic Press; 1986:x–xi.
25. Canny J. A computational approach to edge detection. IEEE Trans Pattern Anal Machine Intell 1986;8:679–98.
26. Hibbard LS, Hawkins RA. Objective image alignment for three-dimensional reconstruction of digital autoradiograms. J Neurosci Methods 1988;26:55–74.
27. Zhao W, Young TY, Ginsberg MD. Registration and three-dimensional reconstruction of autoradiographic images by the disparity analysis method. IEEE Trans Med Imaging 1993;12: 782–91.
28. Goldszal AF, Tretiak OJ, Hand PJ, Bhasin S, McEachron DL. Three-dimensional reconstruction of activated columns from 2-[^{14}C]deoxy-D-glucose data. Neuroimage 1995;2:9–20.
29. Nikou C, Heitz F, Nehlig A, Namer IJ, Armspach JP. A robust statistics-based global energy function for the alignment of serially acquired autoradiographic sections. J Neurosci Methods 2003;124:93–102.
30. Zhao W, Ginsberg MD, Smith DW. Three-dimensional quantitative autoradiography by disparity analysis: theory and application to image averaging of local cerebral glucose utilization. J Cereb Blood Flow Metab 1995;15:552–65.
31. Ginsberg MD, Zhao W, Singer JT, Alonso OF, Loor-Estades Y, Dietrich WD, et al. Computer-assisted image-averaging strategies for the topographic analysis of in situ hybridization autoradiographs. J Neurosci Methods 1996;68:225–33.
32. Rubins DJ, Melega WP, Lacan G, Way B, Plenevaux A, Luxen A, et al. Development and evaluation of an automated atlas-based image analysis method for microPET studies of the rat brain. Neuroimage 2003;20:2100–18.